9th Asia-Pacific Conference on Wind Engineering
Auckland, New Zealand
3-7 December 2017

A LES investigation of flow over two tandem circular cylinders at an intermediate Reynolds number

Qiang Zhou[1], Zhiguo Li[1], Haili Liao[1] And Mingshui Li[1]

[1]Research Center for Wind Engineering,

Southwest Jiaotong University, Chengdu, Sichuan 610031, China

Abstract

Three-dimensional Large Eddy Simulation (LES) was carried out to investigate the flow around pairs of circular cylinders in tandem arrangements at an intermediate Reynolds number, $Re=1\times10^3$. The spacing ratio *L/D* (ratio of center-to-center distance between the two cylinders *L* to cylinder diameter *D*) is varied from 2 to 6 where all the three main flow patterns are included, and the results obtained from simulation are compared with the experimental and numerical results of isolated circular cylinder case. Particular attention is devoted to the time-averaged and instantaneous flow fields, as well as the mean and fluctuating forces, by analyzing the Strouhal number, vortices structures, streamlines, velocity profiles and pressure distributions in order to enhance understanding of flow dynamic interaction between two circular cylinders. In addition, the spanwise correlations of surface pressures on both upstream and downstream cylinders are discussed.

1. Introduction

Many structural and environmental engineering problems, such as fluid-induced vibration, flow-driven dispersion of pollution and acoustic noise, are directly relevant to unsteady flow past cylindrical structures, which motivates the interest of many researchers. In particular, the flows around the pairs of circular cylinders in tandem, side-by-side or staggered arrangements have been extensively studied in the past several decades because of their fundamental and practical importance, and a considerable number of studies have been summarized in comprehensive reviews (Sumner, 2010; Zdravkovich, 1977, 1988; Zhou and Alam, 2016). Despite the large number of studies in the literature, the complexity of the flow around two circular cylinders will continue to motivate further research (Sumner, 2010).

As for the tandem circular cylinders, the flow is highly complicated and sensitive the Reynolds number and the spacing ratio *L/D*, which thus is classified into different regimes to understand the fluid behaviours based on a combination of theory, measurement and observation(Carmo, Meneghini, & Sherwin, 2010; Igarashi, 1981; Xu & Zhou, 2004; Zdravkovich, 1987; Zhou & Yiu, 2006). According to the classification of Zhou and Yiu (2006), similar to that of Zdravkovich (1987) and Carmo et al. (2010), the flow patterns can be divided into three main types of wake interference behaviors: (i) extended-body regime, where spacing ratio is small ($L/D<2$) and the two cylinders act as a single structure, (ii) reattachment regime, where spacing ratio is intermediate ($2<L/D<5$) and the shear layers from the upstream cylinder reattach on the surface of downstream cylinder, (iii) co-shedding regime, where the spacing ratio is larger than critical spacing ratio ($L/D>5$) at which the Karman vortex starts to shed from the upstream cylinder.

Numerous experimental studies of two tandem circular cylinders have been carried out with difference spacing ratios from low Reynolds numbers (e.g. Huhe-Aode and Taneda (1985) at Re=100, 300 with spacing ratio from 1.5 to 10) to supercritical Reynolds numbers (e.g. Gu, Sun, He, and Zhang (1993) at $Re=6.5\times10^5$), in which the number of investigations were undertaken at the intermediate Reynolds numbers, $Re=1.0\times10^3$~1.0×10^4 (e.g. Wu, Welch, Welsh, Sheridan, and Walker (1994) at $Re=1.0\times10^3$, Sumner, Price, and Paidoussis (1999) at $Re=1.2\times10^3$~3.8×10^3, Ozono et al. (2001) at $Re=2.5\times10^3$~7.5×10^3, Lin, Yang, and Rockwell (2002) at $Re=1\times10^4$, Zhou and Yiu (2006) at $Re=7\times10^3$). On the other hand, more and more reported research works on the flow around two circular cylinders are performed by numerical approaches in the last two decades as a result of the rapidly developing computing power. However, most of these numerical studies are two-dimensional or are restricted to low Reynolds numbers ($Re<1000$).

In the present study, the flow around the two tandem circular cylinders with different spacing ratios are investigated by performing three-dimensional Large-Eddy simulations at an intermediate Reynolds number, $Re=1\times10^3$. Five spacing ratio, *L/D*=2, 3, 3.5, 4 and 6, are chosen as the research objects because they cover all the three main flow patterns as described above. Particular attention is devoted to the time-averaged and instantaneous flow fields as well as the mean and fluctuating forces. The numerical method and numerical details applied in this study are first described and verified by presenting the aerodynamics of isolated circular cylinder at Re=3,900, in addition to detailed comparisons of the time-averaged and instantaneous flow fields. Then, we focus on the Strouhal number, time-averaged and instantaneous flow patterns, and pressure distributions on two cylinders, as well as the mean and fluctuating forces. By analyzing the results obtained for two tandem circular cylinders, the underlying mechanism for the variations caused by spacing ratios are studied. Finally, the spanwise correlations of surface pressures are provided.

2. Numerical method

2.1 Problem formulation

We study the flows around the two tandem circular cylinders by performing three-dimensional unsteady simulations of the incompressible governing equations of the fluids. Eqs. (1) and (2) show the filtered continuity and Navier-Stokes equations for Large Eddy Simulation, in which the grid-scale turbulence is solved while the sub-grid-scale turbulence is modeled.

$$\frac{\partial \overline{u_i}}{\partial x_i} = 0 \tag{1}$$

$$\frac{\partial(\overline{u}_i)}{\partial t} + \frac{\partial(\overline{u}_i\overline{u}_j)}{\partial x_j} = -\frac{1}{\rho}\frac{\partial \overline{P}}{\partial x_i} + \nu\frac{\partial^2 \overline{u}_i}{\partial x_j \partial x_j} - \frac{\partial \tau_{ij}}{\partial x_j} \tag{2}$$

where u_i (i=1, 2, 3) are the three velocity components. The over-

bar denotes the space filtered quantities. ρ, P and ν represent the air density, pressure and kinematic viscosity of the flow, respectively. The subgrid scale stresses (SGS stress), $\tau_{ij} = \overline{u_i u_j} - \overline{u_i}\,\overline{u_j}$, are expressed in Eq. (3),

$$\tau_{ij} - \frac{1}{3}\delta_{ij}\tau_{kk} = -2\nu_{SGS}\overline{S}_{ij} = \nu_{SGS}\left(\frac{\partial \overline{u}_i}{\partial x_j} + \frac{\partial \overline{u}_j}{\partial x_i}\right) \quad (3)$$

where $\overline{S}_{ij}$ is the strain rate tensor, ν_{SGS} is the SGS eddy viscosity and

$$\nu_{SGS} = C\overline{\Delta}^2\left|\overline{S}\right| \quad (4)$$

where $\overline{\Delta}$ is the size of grid filter, and based on the Smagorinsky model proposed by Germano, Piomelli, Moin, and Cabot (1991), the following expressions can be derived to solve for the unknown model coefficient C with the contraction obtained from the least square analysis of Lilly (1992) :

$$L_{ij} = \widehat{u_i u_j} - \widehat{u_i}\,\widehat{u_j}$$
$$M_{ij} = -2(\hat{\Delta}^2\left|\widehat{\overline{S}}\right|\widehat{\overline{S}}_{ij} - \Delta^2\widehat{\left|\overline{S}\right|\overline{S}_{ij}})$$
$$C = \frac{(L_{ij} - L_{kk}\delta_{ij}/3)}{M_{ij}M_{ij}} \quad (5)$$

where the symbol $\widehat{\ }$ means the operation of a test filter and the new filter width $\hat{\Delta}$ is is equal to twice the grid filter width Δ. To avoid numerical instability, the negative value of the SGS eddy viscosity is truncated to zero. Large Eddy Simulation using the dynamic Smagorinsky model has been widely utilized as a relatively affordable and easy-to-use approach for simulation of the flow over bluff bodies (e.g. Kravchenko and Moin (2000), Cao, Ozono, Tamura, Ge, and Kikugawa (2010)).

2.2 Numerical discretization and algorithm

In the simulation, the velocity and pressure are defined at the center of a control volume, while the volume fluxes are defined at the midpoint of their corresponding cell surfaces. The Momentum Interpolation Method (MIM) is used to avoid oscillating problems by eliminating the checkerboard pressure and subsequent refinements with non-staggered mesh. The SIMPLE (Semi-Implicit Method for Pressure-Linked Equations) algorithm is utilized, in which governing equations are solved sequentially because of their non-linearity and coupling characteristics and the solution loop is carried out iteratively in order to obtain a converged numerical solution. The pressure field is extracted by solving a pressure correction equation obtained by manipulating continuity and momentum equations, while the velocity field is obtained from the momentum equations.

2.3 Grid system and boundary condition

As shown in Fig. 1, the computational domain is 45D in x-direction, 20D in y-direction and 4D in z-direction. The blockage ratio is 5%, which is smaller than the suggestion (6.4%) of Sohankar (2008). For the spanwise domain length, Tamura et al. (1998) and Norberg (1994) showed that it is necessary to make $L_z/D \geq 1$ (the ratio of spanwise domain length L_z to cylinder diameter D) in order to achieve a good simulation of the mean and RMS of aerodynamic forces on the cylinder. Thus, the spanwise lengths L_z are set to 4D in the present simulation.

The boundary conditions for simulation are as follows

Body surface: A no-slip condition for u_i=0 and a Neumann condition for pseudo-pressure ϕ are imposed.

Inlet: The velocity condition set as u=10m/s, v=0 and w=0, and a Neumann condition of pseudo-pressure ϕ are imposed at the inlet boundary.

Outflow boundary: A convective boundary condition ($\partial\phi/\partial t + \overline{u}\cdot\partial\phi/\partial x = 0$) is applied for velocity, and Neumann condition for pseudo-pressure.

Spanwise: A periodic condition for velocity and pseudo-pressure is applied.

Upper and lower sides: A symmetric condition is applied to both velocity and pseudo-pressure.

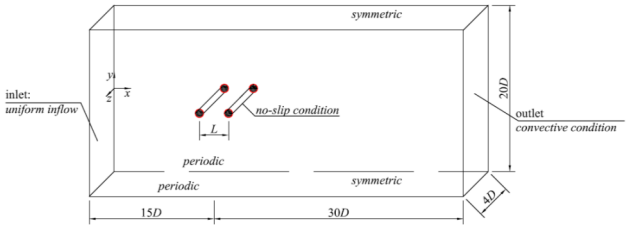

Fig. 1 Computational domain and boundary conditions

Fig. 2 presents the grid near the cylinders in the case of L/D=4. Structured O-type grid systems with the depth of the first grid near the body surface given empirically as $0.1/\mathrm{Re}^{0.5}$ are applied to adequately resolve the flow. For more efficient simulations, the computational domain is spatially resolved such that a dense clustering of grid points is applied near the cylinder, especially in the wake zone, while a coarser grid is used away from the cylinder. Referring to the studies of Tamura et al. (1998) on the influence of spanwise resolution on the simulation results, 25 cells are uniformly distributed. For the temporal discretization, the non-dimensional time-step $\Delta t^* = \Delta t U/D$ (Δt: the time-step for calculation) is 5×10^{-3}, which maintains the Courant Number less than 1.

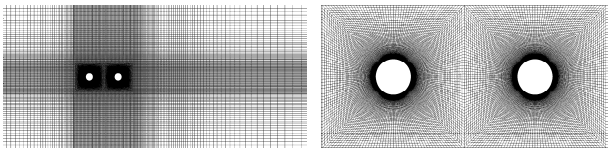

Fig. 2 Close-up view of grid system in the case of L/D=4

3. Numerical validation

To validate the present simulation, basic aerodynamic parameters of the isolated circular cylinder at Re=3900 obtained by present numerical method are compared with those of previous numerical and experimental studies. The flow field around an isolated circular cylinder is utilized as a subject for comparison as shown in Fig.3 and Fig.4. The numerical method and the grid system utilized in the present simulation for isolated circular cylinder provides reasonably good simulation results, which means that the same numerical method and grid system can be applied to the simulation of flow over two tandem circular cylinders.

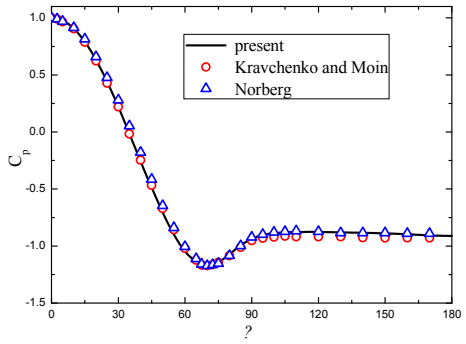

Fig.3 Pressure coefficient on the isolated circular cylinder surface

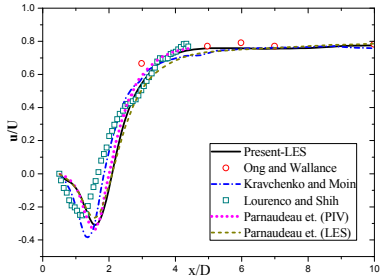

Fig.4 Streamwise velocity on the center line in the wake in the case of isolated circular cylinder

4. Results and discussion

4.1 Flow structures

Fig. 5 show the contours of instantaneous *z*-vorticity at the middle of the cylinder span for the cases of *L/D*=2, 3, 3.5, 4 and 6, where the blue and red colours represent clockwise and counter clockwise vortices, respectively. All these figures correspond to the moment when the lift coefficient is maximum. As for the case of *L/D*=2, the upper side shear layer separated from the upstream cylinder reattached to the downstream one, while the other shear layer on the lower side got over the downstream cylinder and formed a vortex in the wake behind the downstream cylinder. With the development of flow, the lower side shear layer would reattach on the downstream one. It means that the shear layers separated from upstream cylinder reattaches alternately on the downstream cylinder, which is also obtained by Zdravkovich (2003) and Kitagawa and Ohta (2008).

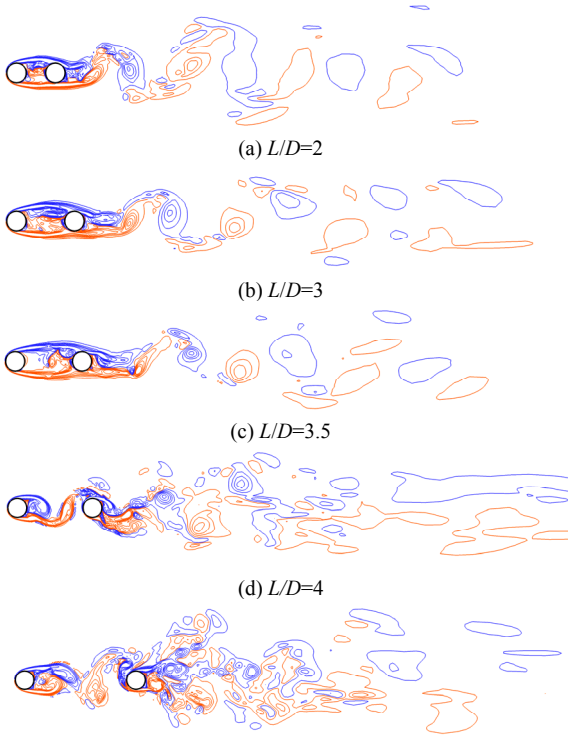

(a) *L/D*=2

(b) *L/D*=3

(c) *L/D*=3.5

(d) *L/D*=4

(e) *L/D*=6

Fig.5 Instantaneous vorticity at middle of cylinder span ($\omega_Z=\pm 2$)

Fig. 6 shows the variation of Strouhal number with spacing ratio at Re=1,000 and compare with those of previous studies, of which Xu and Zhou (2004) is experimental studies at Re=1,200 and 2,900, and Kitagawa and Ohta (2008) is numerical study at Re=22,000. Strouhal number is defined as $St=fD/U$, where vortex shedding frequency f is detected by FFT from the lift force on the cylinder. As for the cases of *L/D*<4, the Strouhal number decreases slowly during the reattachment regime as *L/D* is increased, where the *St* value is lower than the that of an isolated cylinder and reach a minimum value of about *St*=0.145 at Re≈1,000, such as present result of *St*=0.144 at *L/D*=3.5 and *St*=0.147 of Xu and Zhou (2004) at *L/D*=4. Then it can be found obviously that there is a discontinuous jump in Strouhal number at the critical spacing ratio, where the *St* value suddenly increase to *St*=0.187 due to the change of flow pattern. Meanwhile, the same *St* value is observed behind both cylinders, which means that the obvious Karmen vortex shedding are occurred behind both upstream and downstream cylinders. As the spacing ratio increases the value of Strouhal number slowly increases and approaches the value *St*=0.205 at *L/D*=6, which is almost the same as that of isolated cylinder.

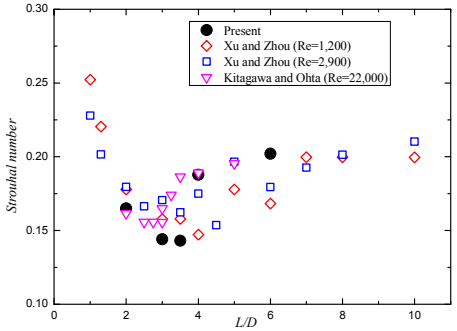

Fig. 6 Variation of Strouhal number with spacing ratio

4.2 Aerodynamic forces

Here the mean and fluctuating drag and lift forces of upstream and downstream cylinders with spacing ratio *L/D*=2, 3.5, 4 and 6 are discussed. As shown in Table 1, it can be found that the mean drag coefficient C_d decreases slowly with increasing *L/D* in the reattachment regime at Re=1,000 as shown in Table 1 and Fig. 8. Then as the spacing ratio is larger than critical value, where the flow pattern changes to the co-shedding regime, the mean drag coefficient $C_{d\text{-}u}$ of upstream cylinder jumps to a higher value $C_d\approx 1.10$ approaching to the value of single cylinder, and the mean drag coefficient $C_{d\text{-}d}$ of downstream cylinder jumps from a smaller negative value to a larger positive value. Similar change is also obtained by the experimental study of Alam et al. (2003) at a subcritical Reynolds number Re=6.5×10^4. It should be mentioned that the obvious disparity of C_d value in the co-shedding regime may be as a result of different Reynolds number.

Table 1 The summary of mean and fluctuating drag coefficients

spacing ratio *L/D*	upstream cylinder		downstream cylinder	
	$C_{d\text{-}u}$	$C'_{d\text{-}u}$	$C_{d\text{-}d}$	$C'_{d\text{-}d}$
2	0.975	0.010	-0.154	0.085
3.5	0.854	0.004	-0.167	0.077
4	1.101	0.104	0.531	0.163
6	1.110	0.059	0.561	0.128

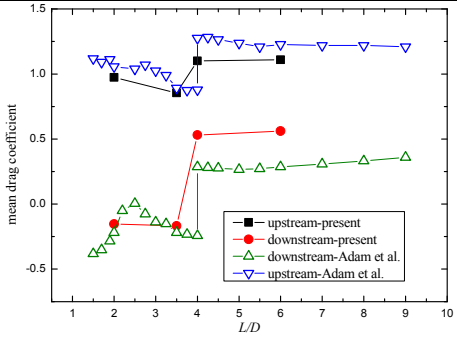

Fig. 7 Variation of mean drag coefficients on cylinders with spacing ratio

As shown in the Fig. 9(a), the fluctuating lift coefficient $C'_{L\text{-}u}$ of the upstream cylinder is smaller that of the downstream cylinder at *L/D*=2. It is because there is no vortex shedding occurs from

the upstream cylinder and fluctuating lift of the upstream cylinder is induced by the movement of side shear layers. However, the fluctuating lift of the downstream cylinder is caused by the vortex shedding, as well as the alternate reattachment of the upstream-cylinder shear layers. As for the case of L/D=3.5, both the amplitudes of the upstream and downstream cylinders are obviously smaller than those in the case of L/D=2 as shown in Fig. 9(b). The reason is that the upstream-cylinder shear layers no longer reattaches alternately on the surface of downstream cylinders. After the critical spacing ratio L/D≥4, the fluctuating lifts on both the upstream and downstream cylinders become obviously larger. The reason for the lift change of upstream cylinder is due to the appearance of vortex shedding from the upstream cylinder, while the reason for the lift change of downstream cylinder is that vortex shedding from upstream cylinder impinge on the downstream cylinder. It can be also observed that the fluctuating lift coefficient of downstream cylinder decreases with the increasing of spacing ratio L/D in the co-shedding regime. This is because the vortex shedding from upstream cylinder impinge stronger on the downstream cylinder when the space between the two cylinders is smaller.

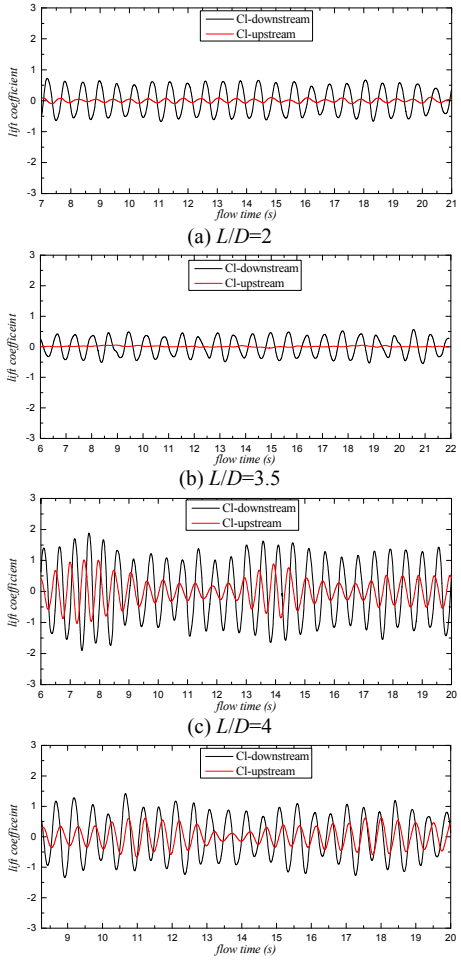

(a) L/D=2

(b) L/D=3.5

(c) L/D=4

(d) L/D=6

Fig. 8 Time histories of lift coefficients

Conclusion remark

1. The three-dimensionality effects of low field around the two tandem circular cylinders are obvious at Re=1000, and the streamwise vortices are found in present simulations.

2. All the three flow patterns of two tandem circular cylinders with spacing ratio ranging from 2 to 6 are observed in present numerical investigation, which include the single bluff body behaviour, shear layer reattachment behaviour and vortex shedding from both cylinders.

3. The relationship between the Strouhal number and spacing ratio L/D agrees reasonably with the previous experimental and numerical results.

4. The mean and the fluctuating pressures were obviously different with the spacing ratio, and as for the fluctuating forces on both the upstream and downstream cylinders, there is an obvious jump at the critical spacing ratio due to the translation of flow pattern.

5. The spanwise correlations of surface pressures on the downstream cylinder decreases as the spacing ratio exceeds the critical value.

Acknowledgments

This research was funded in part by the Natural Science Foundation of China (NSFC, No. 51378442) and the Fundamental Research Funds for the Central Universities (No.2682016CX006).

References

[1] Alam, M.M., Moriya, M., Takai, K., Sakamoto, H., (2003). Fluctuating fluid forces acting on two circular cylinders in a tandem arrangement at a subcritical Reynolds number. *Journal of Wind Engineering and Industrial Aerodynamics*, 91, 139-154.

[2] Cao, S., Ozono, S., Tamura, Y., Ge, Y., & Kikugawa, H. (2010). Numerical simulation of Reynolds number effects on velocity shear flow around a circular cylinder. *Journal of Fluids and Structures,* 26(5), 685-702.

[3] Carmo, B. S., Meneghini, J. R., & Sherwin, S. J. (2010). Secondary instabilities in the flow around two circular cylinders in tandem. *Journal of Fluid Mechanics, 644*, 395-431.

[4] Germano, M., Piomelli, U., Moin, P., & Cabot, W. H. (1991). A dynamic subgrid - scale eddy viscosity model. *Physics of Fluids A: Fluid Dynamics, 3*(7), 1760-1765.

[5] Gu, Z., Sun, T., He, D., & Zhang, L. (1993). Two circular cylinders in high-turbulence flow at supercritical Reynolds number. *Journal of Wind Engineering and Industrial Aerodynamics, 49*(1-3), 379-388.

[6] Huhe-Aode, T. M., & Taneda, S. (1985). Visual studies of wake structure behind two cylinders in tandem arrangement. *Reports Res Inst Appl Mech Kyushu Univ, 32*, 1-20.

[7] Igarashi, T. (1981). Characteristics of the flow around two circular cylinders arranged in tandem: 1st report. *Bulletin of JSME, 24*(188), 323-331.

[8] Kravchenko, A. G., & Moin, P. (2000). Numerical studies of flow over a circular cylinder at Re D= 3900. *Physics of fluids, 12*(2), 403-417.

[9] Lilly, D. K. (1992). A proposed modification of the Germano subgrid - scale closure method. *Physics of Fluids A: Fluid Dynamics, 4*(3), 633-635.

[10] Lin, J.-C., Yang, Y., & Rockwell, D. (2002). Flow past two cylinders in tandem: instantaneous and averaged flow structure. *Journal of Fluids and Structures, 16*(8), 1059-1071.

[11] Sumner, D., Price, S., & Paidoussis, M. (1999). Tandem cylinders in impulsively started flow. *Journal of Fluids and Structures, 13*(7-8), 955-965.

[12] Wu, J., Welch, L., Welsh, M., Sheridan, J., & Walker, G. (1994). Spanwise wake structures of a circular cylinder and two circular cylinders in tandem. *Experimental Thermal and Fluid Science, 9*(3), 299-308.

[13] Xu, G., & Zhou, Y. (2004). Strouhal numbers in the wake of two inline cylinders. *Experiments in Fluids, 37*(2), 248-256.

[14] Zdravkovich, M. (1987). The effects of interference between circular cylinders in cross flow. *Journal of Fluids and Structures, 1*(2), 239-261.

[15] Zhou, Y., & Yiu, M. (2006). Flow structure, momentum and heat transport in a two-tandem-cylinder wake. *Journal of Fluid Mechanics, 548*, 17-48.